Available online at www.sciencedirect.com
SCIENCE DIRECT®
Inorganica Chimica Acta 358 (2005) 331–338
Inorganica Chimica Acta
www.elsevier.com/locate/ica

Structures and properties of octaethylporphinato(phenolate)iron(III) complexes with NH···O hydrogen bonds: modulation of Fe–O bond character by the hydrogen bond

Daisuke Kanamori, Yusuke Yamada, Akira Onoda, Taka-aki Okamura, Seiji Adachi, Hitoshi Yamamoto, Norikazu Ueyama *

Department of Macromolecular Science, Graduate School of Science, Osaka University, 1-1 Machikaneyama-cho, Toyonaka, Osaka 560-0043, Japan

Received 27 July 2004; accepted 6 September 2004
Available online 30 November 2004

Abstract

Iron(III) porphinate complexes of phenolate that have NH···O hydrogen bonds on the coordinating oxygen, [Fe^{III}(OEP){O-2,6-$(RCONH)_2C_6H_3$}] (R = CF_3 (**1**), CH_3 (**3**)) and [Fe^{III}(OEP)(O-2-$RCONHC_6H_4$)] (R = CF_3 (**2**), CH_3 (**4**)) (OEP = 2,3,7,8,12,13,17,18-octaethyl-21*H*, 23*H*-porphinato), were synthesized and characterized as models of heme catalase. The presence of NH···O hydrogen bonds was established by their crystal structures and IR shifts of the amide NH band. The crystal structure of **1** shows an extremely elongated Fe–O bond, 1.926(3) Å, compared to 1.887(2) Å in **2** or 1.848(4) Å in [Fe^{III}(OEP)(OPh)]. The NH···O hydrogen bond decreases an electron donation from oxygen to iron, resulting in a long Fe–O bond and a positive redox potential.

Keywords: Hydrogen bond; Phenolate complexes; Porphyrin complexes; Iron complexes; Catalase; X-ray analysis

1. Introduction

Heme catalases have a high catalytic ability to disproportion harmful hydrogen peroxide with surprisingly high acceleration [1,2]. They have a tyrosinate, which functions as an axial ligand, with double NH···O hydrogen bonds from the arginine guanidinium group [3–9].

The ''push–pull'' concept is generally used to explain the activation of substrates in heme enzymes. The major role of axial ligands is considered to be ''push''. However, we have previously established additional roles of an axial thiolate in P450 model complexes [10–12]. In these complexes, NH···S hydrogen bonds on the axial thiolate modulate the Fe–S bond character and the redox potential of iron. In the case of catalase, the roles of axial phenolate have been poorly investigated because ''pull'' is considered to be predominant in catalytic activity [13]. However, the NH···O hydrogen bonds on the axial phenolate must modulate the Fe–O bond character and the redox potential of iron because of chemical similarity. Computational studies examining the axial phenolate and its hydrogen bonds have recently reported that the NH···O hydrogen bond positively shifts the oxidation potential of the axial ligand and lowers the Fe–O bond order in high-valent states, compound I and II [14,15]. In our previous report, model complexes having NH···O hydrogen bonds on the coordinating phenolate, [Fe^{III}(TPP)(O-2-$CF_3CONHC_6H_4$)] and [Fe^{III}(TPP){O-2,6-$(CF_3CONH)_2C_6H_3$}] (TPP = tetraphenylporphinato), were synthesized [11]. In that study, the positive shift of the redox potential of Fe^{III}/Fe^{II} by the NH···O hydrogen bonds to the coordinating oxygen has been established but modulation of the Fe–O bond character has not.

The present study provides an indepth discussion of the effects of NH···O hydrogen bonds, especially regard-

* Corresponding author. Tel.: +81 6 6850 5449; fax: +81 6 6850 5474.
E-mail address: ueyama@chem.sci.osaka-u.ac.jp (N. Ueyama).

0020-1693/$ - see front matter © 2004 Elsevier B.V. All rights reserved.
doi:10.1016/j.ica.2004.09.014

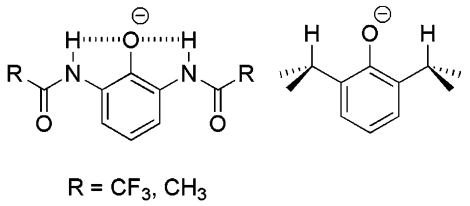

Scheme 1. Phenolate ligands with hydrogen bonds and steric hindrance.

ing Fe–O bond character, by examining what role the number of hydrogen bonds plays and by making a comparison with a steric effect. Various simple 2-mono(acylamino)- and 2,6-bis(acylamino)phenolate ligands were used as models of the axial of catalase. The 2,6-di-isopropylphenolate ligand was also used as non-hydrogen bonding model with a similar bulkiness in order to approximate the steric effect of the acylamino group (Scheme 1). A series of X-ray analyses of novel model complexes with different numbers of hydrogen bonds, [Fe^{III}(OEP){O-2,6-$(CF_3CONH)_2C_6H_3$}], [Fe^{III}(OEP)-(O-2-$CF_3CONHC_6H_4$)], [Fe^{III}(OEP){O-2,6-(*i*-Pr)$_2C_6H_3$}] and [Fe^{III}(OEP)(OPh)] (OEP = 2,3,7,8,12,13,17,18-octaethyl-21*H*,23*H*-porphinato), have been performed. Changes in the Fe–O bond character that appear to be connected to the number of hydrogen bonds were discussed based on a comparison of the structures. Other properties associated with these complexes are also presented in this paper.

2. Experimental

2.1. Materials

All procedures were performed under Ar atmosphere by the Schlenk technique except for ligand syntheses. All organic solvents were dried over CaH_2 and distilled under Ar atmosphere before use. [Fe^{III}(OEP)]$_2$O and [Fe^{III}(OEP)(OPh)] (**5**) were synthesized by the reported method [16]. Other reagents including 2-acetylaminophenol were purchased from Nacalai Tesque or Tokyo Chemical Industry and used without further purification.

2.2. Synthesis of axial ligands

2.2.1. 2,6-Diaminophenol dihydrochloride

2,6-Dinitrophenol (1.5 g, 8.2 mmol) was suspended in concentrated hydrochloric acid (36 ml). Then, tin powder (3.0 g) was added slowly to the mixture with stirring at room temperature. After this solution turned yellow, it was slowly cooled to 4 °C. The obtained white needles were collected and recrystallized from hot water/concentrated hydrochloric acid. Yield: 1.5 g (91%) ^{1}H NMR (DMSO-d_6); δ ppm 9.02 (OH, NH_3), 7.11 (*m*-H), 6.89 (*p*-H).

2.2.2. 2,6-Bis(acetylamino)phenol

To an aqueous solution (10 ml) of 2,6-diaminophenol dihydrochloride (1.8 g, 9.1 mmol), acetic anhydride (3 ml, 32 mmol) and sodium acetate trihydrate (3.5 g, 26 mmol) were added and heated. After cooling down to room temperature, there appeared white needles. Yield: 1.2 g (70%); m.p. 178–179 °C. *Anal.* Calc. for $C_{10}H_{12}N_2O_3$: C, 57.68; H, 5.81; N, 13.45. Found: C, 57.64; H, 5.77; N, 13.41%. ^{1}H NMR (DMSO-d_6); δ ppm 9.99 (OH), 9.70 (NH), 7.40 (*m*-H), 6.82 (*p*-H), 2.18 (CH_3).

2.2.3. 2,6-Bis(trifluoroacetylamino)phenol

To a CH_2Cl_2 solution (20 ml) of 2,6-diaminophenol dihydrochloride (0.5 g, 2.5 mmol), including triethylamine (1.6 ml, 11 mmol), trifluoroacetic anhydride (0.90 ml, 5.6 mmol) was slowly added at 0 °C. After the solution was stirred for 60 min, 10 ml of water was added and then CH_2Cl_2 was removed under reduced pressure. The residue was dissolved in ethyl acetate (100 ml) and the organic layer was washed with 100 ml of water twice. After drying over anhydrous Na_2SO_4, the solution was concentrated. The obtained residue was recrystallized from diethyl ether/*n*-hexane. Yield: 340 mg (42%); m.p. 136–138 °C. *Anal.* Calc. for $C_{10}H_6N_2O_3F_6$: C, 37.99; H, 1.91; N, 8.86. Found: C, 37.84; H, 1.83; N, 9.47%. ^{1}H NMR (DMSO-d_6); δ ppm 10.70 (NH), 9.81 (OH), 7.37 (*m*-H), 6.96 (*p*-H).

2.2.4. 2-Trifluoroacetylaminophenol

2-Trifluoroacetylaminophenol was synthesized from 2-aminophenol in a similar method to 2,6-bis(trifluoroacetylamino)phenol. ^{1}H NMR (DMSO-d_6); δ ppm 10.51 (NH), 9.93 (OH), 7.38 (3-H), 7.20 (5-H), 6.99 (6-H), 6.89 (4-H).

2.3. Synthesis of [Fe^{III}(OEP){O-2,6-$(CF_3CONH)_2C_6H_3$}] (**1**), [Fe^{III}(OEP)(O-2-$CF_3CONHC_6H_4$)] (**2**), [Fe^{III}(OEP){O-2,6-$(CH_3CONH)_2C_6H_3$}] (**3**), [Fe^{III}(OEP)(O-2-$CH_3CONHC_6H_4$)] (**4**), and [Fe^{III}(OEP){O-2,6-(*i*-Pr)$_2C_6H_3$}] (**6**)

[Fe^{III}(OEP)]$_2$O was mixed with corresponding phenol (1 equiv. for **1**–**4** and 5 equiv. for **6**) in CH_2Cl_2 at room temperature. After being stirred for 1 h, the solution was concentrated to dryness. **1** was recrystallized from toluene/*n*-hexane, **2** was from dichloromethane/diethyl ether, **3** and **4** were from toluene, and **6** was from toluene/acetonitrile. **1**–**4** were dark purple crystals and **6** was black.

2.3.1. [Fe^{III}(OEP){O-2,6-$(CF_3CONH)_2C_6H_3$}] (**1**)

Anal. Calc. for $C_{46}H_{49}N_6O_3FeF_6$: C, 61.13; H, 5.46; N, 9.30. Found: C, 60.18; H, 5.30; N, 9.14%. UV/Vis (CH_2Cl_2, r.t.); λ_{max} ($\varepsilon \times 10^{-4}$ cm^{-1} M^{-1}) 625 (6.8), 527

(11.5), 497 (12.0), 384 (110). ^{1}H NMR ($CDCl_3$); δ ppm 71.9 (3-H), −81.6 (4-H), −33.8 (*meso*), 38.7, 42.8 (–CH_2–), 6.1 (–CH_3), 3.6 (NH).

*2.3.2. [Fe^{III}(OEP)(O-2-$CF_3CONHC_6H_4$)] (**2**)*

Anal. Calc. for $C_{44}H_{49}N_5O_2FeF_3$: C, 66.66; H, 6.23; N, 8.83. Found: C, 66.10; H, 6.15; N, 8.77%. UV/Vis (CH_2Cl_2, r.t.); λ_{max} ($\varepsilon \times 10^{-4}$ cm^{-1} M^{-1}) 614 (5.7), 523 (8.52), 496 (8.67), 391 (79.0). ^{1}H NMR ($CDCl_3$); δ ppm −89 (6-H), 90.4 (3-H), 65.4 (5-H), −90.9 (4-H), −35.5 (*meso*), 39.3, 36.4 (–CH_2–), 5.9 (–CH_3).

*2.3.3. [Fe^{III}(OEP){O-2,6-($CH_3CONH)_2C_6H_3$}] (**3**)*

Anal. Calc. for $C_{46}H_{55}N_6O_3Fe \cdot C_7H_8$: C, 71.69; H, 7.15; N, 9.46. Found: C, 71.44; H, 7.16; N, 9.52%. UV/Vis (CH_2Cl_2, r.t.); λ_{max} ($\varepsilon \times 10^{-4}$ cm^{-1} M^{-1}) 617 (7.7), 524 (11.7), 497 (13.2), 392 (117). ^{1}H NMR ($CDCl_3$); δ ppm 83.9 (3-H), −98.5 (4-H), −34.0 (*meso*), 38.5, 36.6 (–CH_2–), 5.7 (–CH_3), 3.3 (NH), 11.6 (acetyl-H).

*2.3.4. [Fe^{III}(OEP)(O-2-$CH_3CONHC_6H_4$)] (**4**)*

Anal. Calc. for $C_{44}H_{52}N_5O_2Fe \cdot (C_7H_8)_{0.25}$: C, 72.13; H, 7.14; N, 9.19. Found: C, 72.30; H, 7.18; N, 9.56%. UV/Vis (CH_2Cl_2, r.t.); λ_{max} ($\varepsilon \times 10^{-4}$ cm^{-1} M^{-1}) 617 (7.7), 524 (11.7), 497 (13.2), 392 (117). ^{1}H NMR ($CDCl_3$); δ ppm −108 (6-H), 96.2 (3-H), 78.5 (5-H), −103.0 (4-H), −34.8 (*meso*), 35.7 (–CH_2–), 5.4 (–CH_3), 3.3 (NH), 9.8 (acetyl-H).

*2.3.5. [Fe^{III}(OEP){O-2,6-(*i*-Pr)$_2C_6H_3$}] (**6**)*

UV/Vis (CH_2Cl_2, r.t.); λ_{max} ($\varepsilon \times 10^{-4}$ cm^{-1} M^{-1}) 593 (16.3), 482 (17.6), 396 (165). ^{1}H NMR ($CDCl_3$); δ ppm 123.4 (3-H), −142.6 (4-H), −42.0 (*meso*), 30.8 (–CH_2–), 5.1 (–CH_3), 1.30, 0.91 (*i*-Pr, CH_3).

2.4. Physical measurements

Visible spectra were recorded in dichloromethane solution on a SHIMADZU UV-3100PC spectrophotometer. ^{1}H NMR spectra were taken on a JEOL EX-270 spectrometer in chloroform-*d* solution at 30 °C. Tetramethylsilane was used as a standard (0 ppm). IR spectra were recorded on a Jasco FT/IR 8300 spectrometer. Samples were prepared as KBr pellets. Electrochemical measurements were carried out using a BAS 100B/W instrument in dichloromethane solution (1 mM) that contained 0.1 M tetra-*n*-butylammonium perchlorate as a supporting electrolyte. $E_{1/2}$ value was referenced to an SCE electrode at room temperature and a value uncorrected for junction potential was obtained.

2.5. pH titration

pK_a measurements were performed in 10 mM aqueous or 10% Triton X-100 aqueous micellar solution at 25 °C. The preparation of micellar solutions is as follows. The same volume of Triton X-100 was added to DMF solution (100 mM) of each sample. This solution was diluted by four times the volume of water. The pH of the solution (10 mM) was determined using a Metrohm 716 DMS titrino, which is combined with Metrohm 728 stirrer and a saturated calomel LL micro pH glass electrode. The saturated calomel glass electrode purchased from Metrohm was calibrated by 0.05 M C_6H_4(COOH)(COOK) buffer (pH 4.01) and 0.025 M KH_2PO_4 and 0.025 M Na_2HPO_4 buffer (pH 6.86).

2.6. Ligand exchange reaction

The ligand exchange reactions were performed in $CDCl_3$ at 30 °C. To a solution of [Fe(OEP)(OPh)] in $CDCl_3$ (0.6 ml, 5 mM), each of **1**–**4** was added in the solid state using small funnel. ^{1}H NMR spectra were measured after storing for 30 min at 30 °C. The exchange ratio was determined by the integrated intensity of the peaks in paramagnetic region. When phenol was added to a solution of **1**–**4**, 500 mM solution of phenol in $CDCl_3$ was added successively via microsyringe. Other conditions were the same to the above experiment.

2.7. X-ray structure determination

Each single crystal of [Fe^{III}(OEP){O-2,6-($CF_3CONH)_2C_6H_3$}] (**1**), [Fe^{III}(OEP)(O-2-$CF_3CONHC_6H_4$)] (**2**), [Fe^{III}(OEP)(OPh)] (**5**), and [Fe^{III}(OEP){O-2,6-(*i*-Pr)$_2C_6H_3$}] (**6**) was sealed in a glass capillary under argon atmosphere for the X-ray measurement, which was performed at 23 °C on a Rigaku AFC5R diffractometer equipped with a rotating anode X-ray generator. The radiation used was Mo Kα monochromatized with graphite (0.71069 Å). An empirical absorption correction was applied. The basic crystallographic parameters for **1**, **2**, **5**, and **6** are listed in Table 1. Unit cell dimensions were refined with 25 reflections. These standard reflections were chosen and monitored with every 150 reflections and did not show any significant change. The structure was solved by heavy atom Patterson methods (PATTY [17]) for **1**, **2**, and **5** or a direct method (SHELXS-86 [18]) for **6** and expanded using Fourier techniques. Non-hydrogen atoms were refined anisotropically. Hydrogen atoms were placed at calculated positions. All calculations were performed using the teXsan crystallographic software [1] and SHELXL-97 [19].

[1] Crystal Structure Analysis Package, Molecular Structure Corporation, 1985 and 1992.

Table 1
Crystallographic data for [Fe^{III}(OEP){O-2,6-$(CF_3CONH)_2C_6H_3$}] (**1**), [Fe^{III}(OEP)(O-2-$CF_3CONHC_6H_4$)] (**2**), [Fe^{III}(OEP)(OPh)] (**5**), and [Fe(OEP){O-2,6-(*i*-Pr)$_2C_6H_3$}] (**6**)

	1	**2**	**5**	**6**
Chemical formula	$C_{46}H_{49}O_3N_6FeF_6$	$C_{44}H_{49}O_2N_5FeF_3$	$C_{42}H_{49}ON_4Fe$	$C_{48}H_{61}ON_4Fe$
Formula weight	903.77	792.75	681.72	765.88
Color	black	black	black	black
Crystal system	monoclinic	triclinic	triclinic	orthorhombic
Lattice parameter				
a (Å)	14.298(4)	13.926(3)	12.119(4)	18.988(3)
b (Å)	18.765(4)	14.868(3)	15.122(4)	25.312(3)
c (Å)	17.462(4)	10.053(3)	10.834(3)	18.142(3)
α (°)	90	99.74(2)	97.65(2)	90
β (°)	108.80(2)	103.16(2)	101.35(3)	90
γ (°)	90	94.14(2)	111.05(2)	90
V (Å^3)	4435(1)	1984.4(8)	1771(1)	8719(2)
Space group	$P2_1/n$ (#14)	$P\bar{1}$ (#2)	$P\bar{1}$ (#2)	*Pbca* (#61)
Z	4	2	2	8
D_{calc} (g cm^{-3})	1.353	1.327	1.278	1.167
μ (Mo Kα) (cm^{-1})	4.12	4.37	4.64	3.84
Temperature (K)	296	296	296	296
Scan type	ω–2θ	ω–2θ	ω–2θ	ω–2θ
$2\theta_{max}$ (°)	52.0	55.0	50.0	47.0
R_1	0.051	0.043	0.057	0.051
wR_2	0.143	0.132	0.183	0.161
Number of reflections (total)	9365	9482	6573	7079
Measured (unique)	8997	9108	6249	7079
Number of observations [$I > 3\sigma(I)$]	2824	5319	2730	2359
Goodness-of-fit	0.95	1.03	0.96	0.92

3. Results and discussion

3.1. Molecular structures

The molecular structures of **1, 2, 5**, and **6** are shown in Fig. 1. The crystal parameters of these complexes are listed in Table 1, and the selected bond lengths and angles are listed in Table 2. No significant intermolecular interaction was detected in any of these cases. The amide NH protons in **1** and **2** direct toward the coordinating oxygen. Short distances between the coordinating oxygen and the amide NH protons (2.31 and 2.33 Å in **1** and 2.25 Å in **2**) suggest the existence of NH···O hydrogen bonds. The presence of hydrogen bonds was confirmed using IR spectra as discussed below.

The Fe–O bond length of the NH···O hydrogen bonded complexes (1.926(3) Å for **1** and 1.887(2) Å for **2**) is elongated by 0.039 Å in proportion to the number of hydrogen bonds compared to that of the unsubstituted phenolate complex (**5**), 1.848(4) Å. The Fe–O bond length in **1** is extremely long compared with other reported complexes (1.847–1.868 Å) [11,20–22]. On the other hand, the Fe–O bond length of non-hydrogen-bonded complex with similar bulkiness (**6**) is short (1.816(4) Å), although **6** has methyne CH protons in a similar situation to the NH protons in **1** and **2**. The elongation of the Fe–O bond in **1** and **2** is attributed to the NH···O hydrogen bonds rather than to steric hindrance. These results indicate that the NH···O hydrogen bonding decreases an electron donation from the coordinating oxygen to iron. Fe–N_4 plane distances were shortened by the NH···O hydrogen bond. The short Fe–N_4 plane distance shows that the iron has a low electron density and behaves like a high-valent state in the hydrogen-bonded complexes. If the elongation of the Fe–O bond was caused by the steric hindrance, the Fe–N_4 plane distances must be elongated as well as Fe–O bond lengths [23]. A shortening of the Fe–N_4 plane distances was also observed in P450 model complexes [10,12]. In contrast to the large Fe–O–C bond angle (170.6(4)°, nearly straight) of **6**, the Fe–O–C bond angles of **1**, **2**, and **5** are 122.8(3)°, 125.5(2)°, and 142.2(3)°, respectively. In terms of orbital overlapping, a small Fe–O–C bond angle is not suitable. The small Fe–O–C bond angles in **1** and **2** are probably geometrically favorable to form the NH···O hydrogen bonds in place of orbital overlapping. The elongated Fe–O bond lengths and the small Fe–O–C bond angles show that the NH···O hydrogen bonds reduce the *s*-character of the coordinating oxygen.

3.2. Detection of NH···O hydrogen bonds using IR spectroscopy

Hydrogen bonds in doubly (**1**) and singly (**2**) hydrogen-bonded complexes were established by a shift of the NH band in IR spectra. The ν(NH) bands of **1** and the corresponding phenol were observed at 3379

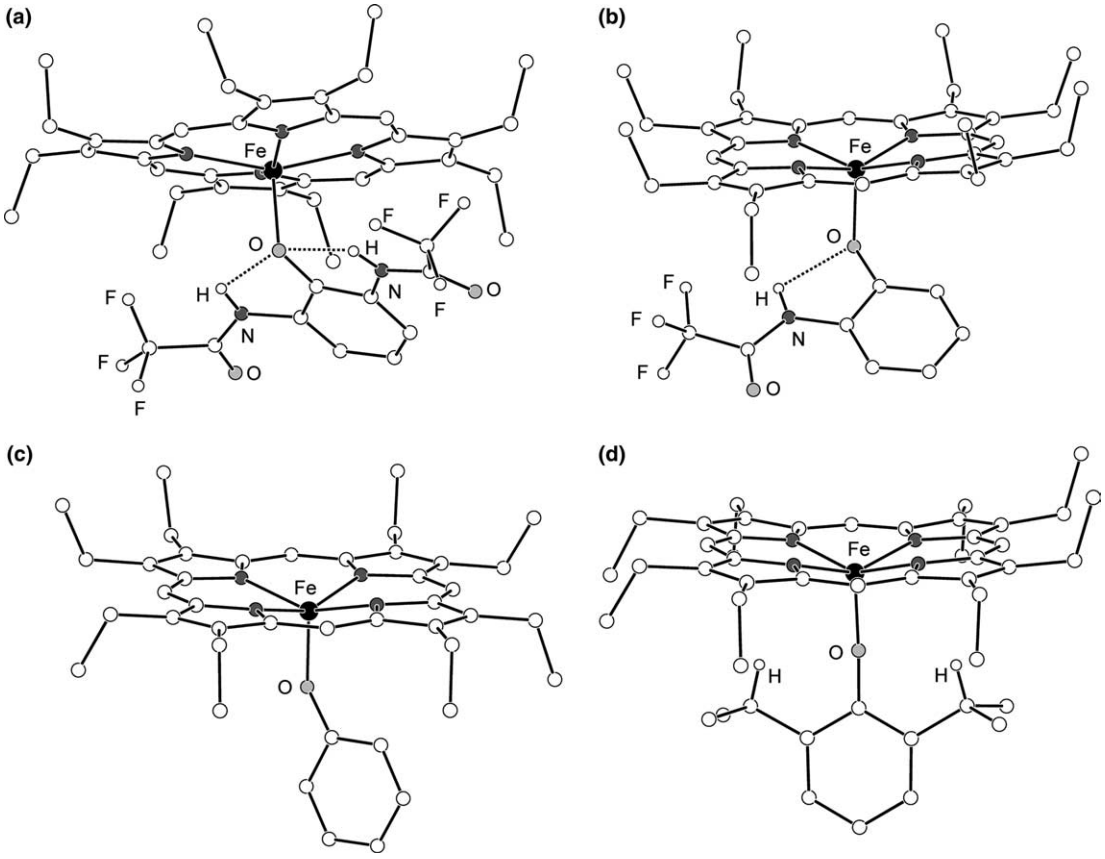

Fig. 1. Molecular structures of: (a) [Fe(OEP){O-2,6-$(CF_3CONH)_2C_6H_3$}] (**1**); (b) [Fe(OEP)(O-2-$CF_3CONHC_6H_4$)] (**2**); (c) [Fe(OEP)(OPh)] (**5**); (d) [Fe(OEP){O-2,6-$(i\text{-}Pr)_2C_6H_3$}] (**6**). Hydrogen atoms except for amide NH and methyne CH are omitted for clarity.

Table 2
Selected bond lengths and angles of [Fe^{III}(OEP){O-2,6-$(CF_3CONH)_2C_6H_3$}] (**1**), [Fe^{III}(OEP)(O-2-$CF_3CONHC_6H_4$)] (**2**), [Fe^{III}(OEP)(OPh)] (**5**), and [Fe(OEP){O-2,6-$(i\text{-}Pr)_2C_6H_3$}] (**6**)

	1	**2**	**5**	**6**
Fe–O (Å)	1.926(3)	1.887(2)	1.848(4)	1.816(4)
Fe–O–C (°)	122.8(3)	125.5(2)	142.2(3)	170.6(4)
Fe–O–C–C (°)	92	113	168	98
Fe–N_{ip} (Å) (mean)	2.051	2.060	2.061	2.071
N–H···O for **1**, **2** or CH···O for **6** (Å)	2.31, 2.33	2.25		2.32, 2.34
Fe to N_{ip} plane (Å)	0.427	0.443	0.467	0.484

and 3390 cm^{-1}, respectively. The low-wavenumber shift of ν(NH) (11 cm^{-1}) supports the suggestion that **1** has NH···O hydrogen bonds, as indicated by X-ray analysis. Similarly, the ν(NH) band of **2** at 3359 cm^{-1} is lower than that of the corresponding phenol, 3388 cm^{-1}. The larger shift of ν(NH) in **2** (29 cm^{-1}) as compared with the shift in **1** indicates the formation of a stronger NH···O hydrogen bond in **2**. This finding is consistent with the results obtained from studying [(TPP)Fe^{III} {O-2,6-$(CF_3CONH)_2C_6H_3$}] and [(TPP)Fe^{III}(O-2-CF_3 $CONHC_6H_4$)], where a single NH···O hydrogen bond is stronger than double hydrogen bonds [11].

The P450 model complexes that have NH···S hydrogen bonds, [Fe(OEP){S-2,6-$(RCONH)_2C_6H_3$}] and [Fe(OEP)(S-2-$RCONHC_6H_4$)] (R = CF_3, CH_3), show a larger shift of ν(NH), 54–123 cm^{-1} [12]. The results show that the NH···S hydrogen bond is stronger than the NH···O hydrogen bond. Even though NH···O hydrogen bonds are weaker, the elongation of the Fe–O bond (0.078 Å) is larger than that of the Fe–S bond (0.057 Å) by NH···S hydrogen bonds. The coordinating sulfur has a low *s*-character even in a non-hydrogen bonded complex, [Fe(OEP)(SPh)], as suggested by a small Fe–S–C bond angle (102.5(3)°). Elongation of the Fe–O or Fe–S bond length depends on not only a decline in the electron donation from the ligand to iron but also a decline in the *s*-character of the coordinating atom. In P450 model complexes, the Fe–S bond length

mostly depends on electron donation because the Fe–S–C bond angles indicate that the *s*-character of the coordinating sulfur exhibits no significant change as a result of the introduction of the NH···S hydrogen bonds. This is because the elongation of the Fe–O bond is larger than that of the Fe–S bond.

3.3. ^1H NMR spectra

Table 3 lists the ^1H NMR chemical shifts of complexes **1**–**6** in chloroform-d at 30 °C. The general pattern of the chemical shifts of phenolate ligand, which does not seem to be affected by a spatial proximity to iron, is described as follows: The *ortho*- and *para*-protons show upfield shifts, whereas *meta*-protons show downfield shifts [24,25]. The alternating shift pattern, which is the opposite sign of the chemical shifts for *meta*- versus *ortho*- and *para*-protons, is indicative of π spin delocalization on the phenolate ligand. If the general pattern was followed, the amide NH protons of **1**–**4** should appear downfield. However, the amide NH protons did not show significant downfield shifts but instead appeared at 3.3–3.6 ppm, slightly upfield compared to the corresponding phenol. This upfield shift has been observed in P450 model complexes that have NH···S hydrogen bonds and has been explained by a direct through NH···S hydrogen bond contact [12]. The results show the NH···O hydrogen bonding in **1**–**4**.

The contact shifts of aryl protons in **1**–**4** are significantly smaller than in the non-hydrogen-bonded complex (**6**). The small contact shifts in **1**–**4** are because of the weakened Fe–O bond by the NH···O hydrogen bonds, which was found as the elongated Fe–O bond in the crystal structure.

3.4. pK_a values of the axial ligand in aqueous solutions and aqueous micellar solutions

It has been reported that pK_a values of axial ligands influence various characteristics of Fe(III) porphinato complexes, namely absorption maxima [26], equilibrium constant of ligand exchange reaction [26,27], and redox potentials [28]. In an aqueous Triton X-100 micellar solution, the pK_a values of 2,6-(*t*-BuCONH)$_2$C$_6$H$_3$OH, 2-*t*-BuCONHC$_6$H$_4$OH and 4-*t*-BuCONHC$_6$H$_4$OH were determined (9.1, 9.6, and 10.1, respectively). Under hydrophobic conditions, the pK_a value of a phenol derivative decreases in the presence of an NH···O hydrogen bond. The hydrophobic conditions used here realize the inside of catalase where the heme group exists. pK_a values in the hydrophobic environments are important because they are affected by the permittivity of the surroundings. The results show that the neighboring amide groups to phenolic OH increase the acidity of the phenolic OH as a result of NH···O hydrogen bond formation during and after deprotonation. This effect of neighboring amide groups has been reported in our previous papers on thiophenol and benzoic acid derivatives [29,30]. Even in an aqueous solution, neighboring amide groups decrease the pK_a value of phenolic OH. For example, we found the pK_a values of 2,6-(CH$_3$CONH)$_2$C$_6$H$_3$OH and unsubstituted phenol in an aqueous 0.1 M NaClO$_4$ solution at 25 °C to be 8.4 and 9.8, respectively. A low pK_a value indicates that a stabilization of the phenolate anion by delocalization of the negative charge on phenolate oxygen has occurred. This finding is consistent with previous discussions, where the NH···O hydrogen bond decreases the electron-donating ability of the coordinating oxygen.

3.5. Ligand exchange reaction detected by ^1H NMR

The ligand exchange reaction, defined as Eq. (1), between [Fe(OEP)(OAr)] and 10 equivalent PhOH was monitored in CDCl$_3$ solution at 30 °C. The equilibrium constants (K) for **1**–**4** are summarized in Table 4. The reaction was monitored based on the integral intensity of *meta*- or 3,5-aromatic protons' signals, and the order of K was determined to be **4** ≫ **2** > **3** > **1**. The results indicate that strongly NH···O hydrogen-bonded com-

Table 3
^1H NMR chemical shifts of [Fe^{III}(OEP)(OAr)] in CDCl$_3$ at 30 °C

	3-H[a] 5-H	4-H	6-H [b]	*meso*	–CH$_2$–	–CH$_3$	NH	COCH$_3$	CH(CH$_3$)$_2$	CH(CH$_3$)$_2$
1	71.9	−81.6		−33.8	38.7 42.8	6.1	3.6			
2	90.4 65.4	−90.9	−89	−35.3	39.3 36.4	5.9	[c]			
3	83.9	−98.5		−34.0	38.5 36.6	5.7	3.3	11.6		
4	96.2 78.5	−103.0	−108	−34.8	35.7	5.4	3.3	9.8		
6	123.4	−142.6		−42.0	30.8	5.1			[c]	1.30, 0.91

[a] The peaks for 3-H and 5-H were distinguished by the difference of their longitudinal relaxation time (T_1).
[b] The peak for 6-H was also observed utilizing the difference of T_1 from that of the 4-H.
[c] Not detected.

Table 4
Equilibrium constants between [Fe(OEP)(OAr)] and [Fe(OEP)(OPh)] in $CDCl_3$ at 30 °C ([Fe] = 5 mM, $[PhOH]_0$ = 50 mM)

[Fe(OEP)(OAr)]	K
[Fe^{III}(OEP){O-2,6-$(CF_3CONH)_2C_6H_3$}] (**1**)	2.56×10^{-4}
[Fe^{III}(OEP)(O-2-$CF_3CONHC_6H_4$)] (**2**)	7.09×10^{-3}
[Fe^{III}(OEP){O-2,6-$(CH_3CONH)_2C_6H_3$}] (**3**)	1.66×10^{-3}
[Fe^{III}(OEP)(O-2-$CH_3CONHC_6H_4$)] (**4**)	>10[3a]

[a] Completely converted to [Fe(OEP)(OPh)] under this condition.

plexes have a smaller K value than weakly hydrogen-bonded ones and that doubly NH···O hydrogen-bonded complexes have a smaller K value than singly NH···O hydrogen-bonded ones. The results show that the NH···O hydrogen bonds support complexation and are consistent with our previous findings concerning ferredoxin model complexes [31].

$$[Fe^{III}(OEP)(OAr)]+PhOH \overset{K}{\rightleftharpoons} [Fe^{III}(OEP)(OPh)]+ArOH$$
$$K=\frac{[Fe^{III}(OEP)(OPh)][ArOH]}{[Fe^{III}(OEP)(OAr)][PhOH]} \quad (1)$$

3.6. Electronic absorption spectra and electrochemical properties

The maxima in the electronic absorption spectra of the complexes, **1**–**6**, are listed in Table 5. All spectra show four absorption maxima in the range from 380 to 650 nm and one shoulder around 360 nm. It has been reported that the wavelength of absorption maxima of (OEP)Fe(III) phenolate complexes is proportional to the acidity of the axial phenolate ligand [26]. In particular, the maximum around 600 nm is sensitive to the acidity. The maxima of NH···O hydrogen-bonded complexes (**1**–**4**) were observed in longer wavelengths than that of non-hydrogen-bonded complexes (**5** and **6**) and shifted to longer wavelengths in proportion to the strength or number of NH···O hydrogen bonds.

The correlation between the redox potentials of [Fe^{III}(OEP)(phenolato)] and the acidity of 4-substituted phenol has also been reported [28]. The phenolate complex, which has a more acidic phenol as an axial ligand, has a more positive Fe^{III}/Fe^{II} redox potential. The redox potentials of **1**–**6** in CH_2Cl_2 at room temperature are summarized in Table 6. As previously determined with NH···S hydrogen bonds [10–12,31], the NH···O hydrogen bonds also shift the Fe^{III}/Fe^{II} redox potentials to the positive side. Although the redox couples of Fe^{III}/Fe^{II} in **1** are irreversible, a process that occurs most likely because of bond dissociation of the weakened Fe–O bond during reduction, the positively shifted reduction potential of the ferric species supports the positive shift of the redox potential. The results show that the NH···O hydrogen bonds decrease the electron density on iron as a result of decreasing the electron donation from the coordinating oxygen to iron.

Table 5
Absorption maxima of [Fe^{III}(OEP)(OAr)] in CH_2Cl_2 at room temperature

			λ_{max} ($\varepsilon\times10^{-4}$/cm^{-1} M^{-1})	
1	625 (6.8)	527 (11.5)	497 (12.0)	384 (110)
2	614 (5.7)	523 (8.52)	496 (8.67)	391 (79.0)
3	617 (7.7)	524 (11.7)	497 (13.2)	392 (117)
4	611 (7.3)	519 (11.2)	494 (11.1)	393 (110)
5[a]	603 (8.23)	520 (10.77)	490 (12.21)	
6	593 (16.3)		482 (17.6)	396 (165)

[a] Ref. [26].

Table 6
Redox potentials of [$Fe^{III/II}$(OEP)(OAr)] vs. SCE in CH_2Cl_2

	E_{pc}	E_{pa}	$E_{1/2}$
1	−0.71	ca. −0.15[a]	ca. −0.43[a]
2	−0.74	−0.49	−0.61
3	−0.81	−0.38	−0.59
4	−0.82	−0.58	−0.70
5			−0.75[b]
6	−0.91	−0.84	−0.88

[a] Tentatively assigned by poor shape.
[b] Ref. [28].

4. Conclusions

The NH···O hydrogen bonding effects were determined to elongate the Fe–O bond and decrease the *s*-character of the coordinating oxygen. The effects are caused by a delocalization of the negative charge on the coordinating oxygen by the hydrogen bonds and leads to a positive shift of redox potential. The presence of the NH···O hydrogen bonds induces significant changes in various properties, although the direction of the NH group toward the coordinating oxygen in model complexes is not very suitable for hydrogen bonding. In catalase, the NH···O hydrogen bond should be more effective than in model complexes because the NH protons of the guanidinium group in catalase direct to a lone pair of the coordinating oxygen in a more suitable orientation.

Appendix A. Supplementary material

Crystallographic data for the structural analysis have been deposited with the Cambridge Crystallographic Data Centre, CCDC Nos. 245729–245732 for compounds **1**, **2**, **5**, and **6**. Copies of this information may be obtained free of charge from The Director, CCDC, 12 Union Road, Cambridge, CB2 1EZ, UK (fax: +44 1223 336 033; e-mail: deposit@ccdc.cam.ac.uk or

www.ccdc.cam.ac.uk). Supplementary data associated with this article can be found, in the online version, at doi:10.1016/j.ica.2004.09.014.

References

[1] H. Sies, Angew. Chem. Int. Ed. 13 (1974) 706.
[2] G.R. Schonbaum, B. Chance, Enzymes, third ed., vol. 13, 1976, p. 363.
[3] I. Fita, A. Silva, M.R.N. Murthy, M.G. Rossmann, Acta Crystallogr. Sect. B: Struct. Sci. B42 (1986) 497.
[4] G.N. Murshudov, W.R. Melik-Adamyan, A.I. Grebenko, V.V. Barynin, A.A. Vagin, B.K. Vainshtein, Z. Dauter, K.S. Wilson, FEBS Lett. 312 (1992) 127.
[5] J. Bravo, N. Verdaguer, J. Tormo, C. Betzel, J. Switala, P.C. Loewen, I. Fita, Structure (London) 3 (1995) 491.
[6] P. Gouet, H.-M. Jouve, O. Dideberg, J. Mol. Biol. 249 (1995) 933.
[7] G.N. Murshudov, A.I. Grebenko, V. Barynin, Z. Dauter, K.S. Wilson, B.K. Vainshtein, W. Melik-Adamyan, J. Bravo, J.M. Ferrán, J.C. Ferrer, J. Switala, P.C. Loewen, I. Fita, J. Biol. Chem. 271 (1996) 8863.
[8] M.J. Máte, M. Zamocky, L.M. Nykyri, C. Herzog, P.M. Alzari, C. Betzel, F. Koller, I. Fita, J. Mol. Biol. 286 (1999) 135.
[9] C.D. Putnam, A.S. Arvai, Y. Bourne, J.A. Tainer, J. Mol. Biol. 296 (2000) 295.
[10] N. Ueyama, N. Nishikawa, Y. Yamada, T. Okamura, A. Nakamura, J. Am. Chem. Soc. 118 (1996) 12826.
[11] N. Ueyama, N. Nishikawa, Y. Yamada, T. Okamura, A. Nakamura, Inorg. Chim. Acta 283 (1998) 91.
[12] N. Ueyama, N. Nishikawa, Y. Yamada, T. Okamura, S. Oka, H. Sakurai, A. Nakamura, Inorg. Chem. 37 (1998) 2415.
[13] W. Melik-Adamyan, J. Bravo, X. Carpena, J. Switala, M.J. Máte, I. Fita, P.C. Loewen, Proteins 44 (2001) 270.
[14] C. Rovira, I. Fita, J. Phys. Chem. B 107 (2003) 5300.
[15] M.T. Green, J. Am. Chem. Soc. 123 (2001) 9218.
[16] J.W. Buchler, H.H. Schneehage, Z. Naturforsch. B 28 (1973) 433.
[17] P.T. Beurskens, G. Admiral, G. Beurskens, W.P. Bosman, S. Garcia-Granda, R.O. Gould, J.M.M. Smits, C. Smykalla, The DIRDIF Program System, Technical Report of the Crystallography Laboratory, University of Nijmegen, The Netherlands, 1992.
[18] G.M. Sheldrick, in: G.M. Sheldrick, C. Kruger, R. Goddard (Eds.), Crystallographic Computing 3, Oxford University Press, Oxford, 1985, p. 175.
[19] G.M. Sheldrick, SHELXL-97: Program for the Refinement of Crystal Ed., University of Göttingen, Germany, 1997.
[20] H.M. Goff, E.T. Shimomura, Y.J. Lee, W.R. Scheidt, Inorg. Chem. 23 (1984) 315.
[21] M.P. Byrn, C.J. Curtis, Y. Hsiou, S.I. Khan, P.A. Sawin, S.K. Tendick, A. Terzis, C.E. Strouse, J. Am. Chem. Soc. 115 (1993) 9480.
[22] A.M. Helms, W.D. Jones, G.L. McLendon, J. Coord. Chem. 23 (1991) 351.
[23] W.R. Scheidt, D.K. Geiger, Y.J. Lee, C.A. Reed, G. Lang, J. Am. Chem. Soc. 107 (1985) 5693.
[24] R.D. Arasasingham, A.L. Balch, R.L. Har, L. Latos-Grazyński, J. Am. Chem. Soc. 112 (1990) 7566.
[25] R.D. Arasasingham, A.L. Balch, C.R. Cornman, J.S. De Ropp, K. Eguchi, G.N. La Mar, Inorg. Chem. 29 (1990) 1847.
[26] T. Uno, K. Hatano, Y. Nishimura, Y. Arata, Inorg. Chem. 29 (1990) 2803.
[27] M.W. Nee, J.R. Lindsay Smith, J. Chem. Soc., Dalton Trans. (1999) 3373.
[28] H. Sugimoto, N. Ueda, M. Mori, Bull. Chem. Soc. Jpn. 55 (1982) 3468.
[29] N. Ueyama, M. Inohara, A. Onoda, T. Ueno, T. Okamura, A. Nakamura, Inorg. Chem. 38 (1999) 4028.
[30] A. Onoda, Y. Yamada, J. Takeda, Y. Nakayama, T. Okamura, M. Doi, H. Yamamoto, N. Ueyama, Bull. Chem. Soc. Jpn. 77 (2004) 321.
[31] N. Ueyama, Y. Yamada, T. Okamura, S. Kimura, A. Nakamura, Inorg. Chem. 35 (1996) 6473.